

Article

Optimal Multi-Sensor Obstacle Detection System for Small Fixed-Wing UAVs

Marta Portugal and André C. Marta * 

IDMEC, Instituto Superior Técnico, Universidade de Lisboa, Av. Rovisco Pais, 1, 1049-001 Lisboa, Portugal;
marta.portugal@tecnico.ulisboa.pt

* Correspondence: andre.marta@tecnico.ulisboa.pt

Abstract: The safety enhancement of small fixed-wing UAVs regarding obstacle detection is addressed using optimization techniques to find the best sensor orientations of different multi-sensor configurations. Four types of sensors for obstacle detection are modeled, namely an ultrasonic sensor, laser rangefinder, LIDAR, and RADAR, using specifications from commercially available models. The simulation environment developed includes collision avoidance with the Potential Fields method. An optimization study is conducted using a genetic algorithm that identifies the best sensor sets and respective orientations relative to the UAV longitudinal axis for the highest obstacle avoidance success rate. The UAV performance is found to be critical for the solutions found, and its speed is considered in the range of 5–15 m/s with a turning rate limited to 45°/s. Forty collision scenarios with both stationary and moving obstacles are randomly generated. Among the combinations of the sensors studied, 12 sensor sets are presented. The ultrasonic sensors prove to be inadequate due to their very limited range, while the laser rangefinders benefit from extended range but have a narrow field of view. In contrast, LIDAR and RADAR emerge as promising options with significant ranges and wide field of views. The best configurations involve a front-facing LIDAR complemented with two laser rangefinders oriented at ±10° or two RADARs oriented at ±28°.

Keywords: sense and avoidance; collision avoidance; optimization; ultrasonic sensor; laser rangefinder; LIDAR; RADAR



Citation: Portugal, M.; Marta, A.C. Optimal Multi-Sensor Obstacle Detection System for Small Fixed-Wing UAVs. *Modelling* **2024**, *5*, 16–36. <https://doi.org/10.3390/modelling5010002>

Academic Editor: Ivano Benedetti and Ivan Dimov

Received: 12 October 2023

Revised: 8 December 2023

Accepted: 12 December 2023

Published: 20 December 2023



Copyright: © 2023 by the authors. Licensee MDPI, Basel, Switzerland. This article is an open access article distributed under the terms and conditions of the Creative Commons Attribution (CC BY) license (<https://creativecommons.org/licenses/by/4.0/>).

1. Introduction

Unmanned Aerial Vehicles (UAVs) have received considerable attention in a myriad of operations due to their enhanced stability and endurance. Despite being initially developed for military purposes [1], there has been a notable upsurge in the civilian market for UAVs [2]. A survey on the safety aspects of civilian drones concluded that UAVs present a high collision risk across most applications [3]. Due to their ability to work in a collaborative and cooperative manner, swarms of drones are typically used for surveillance purposes, i.e., tracking and localizing objects, and this is reflected in another survey [4]. One of the most significant challenges regarding the navigation of a swarm of agents is collision avoidance [5]. Collision avoidance systems are responsible for guiding an autonomous agent to safely and reliably avoid potential collisions with other agents in the swarm, as well as with other objects in the environment. The capacity to locally sense and avoid items in the environment becomes more crucial for agents to be fully autonomous and, in turn, for systems to be more robust. Drones are also required to exhibit a practical resolution for a Sense and Avoid feature as part of the NextGen [6] strategy for integrating UAVs into the U.S. National Airspace System (NAS). In fact, all UAVs must deploy an automated Sense and Avoid intelligent system that provides safety levels comparable to, or even superior to, those of manned aircraft [7].

Fittingly, this work specifically addresses the safety enhancement of small fixed-wing UAVs (a maximum take-off weight of <25 kg, a range of <10 km, an endurance of <2 h,

and a flight altitude of <120 m), particularly with regard to the detection of obstacles during flight and the automatically triggered collision avoidance maneuver. In contrast to rotary-wing UAVs (multirotors), whose hovering capabilities facilitate collision avoidance strategies and for which many solutions are available, fixed-wing UAVs (conventional aircraft with unmovable lifting surfaces) pose a greater challenge and fewer solutions exist for it.

This work aims to address parts of a comprehensive obstacle detection and collision avoidance system, thereby representing a two-stage “sense” and “avoid” problem. The generic Sense and Avoidance (S&A) system architecture is depicted in Figure 1. Notice that the outcome of the system is to feed updated flight trajectory information to the flight controller, such that the UAV can continue to navigate safely. This all starts with the sensing system, so its definition and performance are critical.

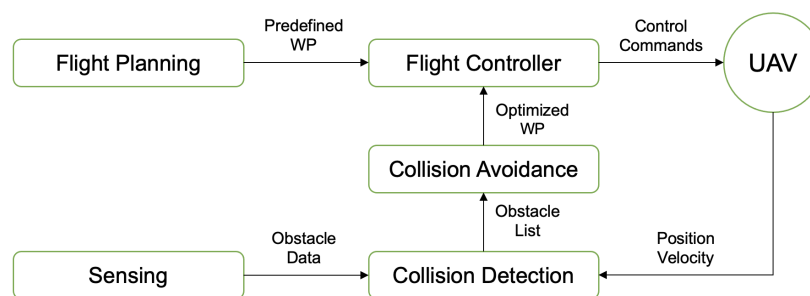


Figure 1. Sense and avoidance system architecture.

In this study, the sensors used to gather obstacle data are the ultrasonic sensor, laser rangefinder, Light Detection and Ranging (LIDAR) sensor, and Radio Detection and Ranging (RADAR) sensor.

Ultrasonic sensors generate sound waves, which are then reflected by the obstacle and recorded by the sensor. In knowing the speed of the radiated sound in the air medium, the distance from the point of greatest reflection to the obstacle can be calculated. Using these sensors proves to be advantageous mainly due to the ease at which this simple technology can be sized down, which is why ultrasonic-based systems were proposed for a similar application [8]. However, because these are proximity sensors, their signal quickly attenuates and their capacity to measure distance is typically limited to less than 10 m [9].

Laser rangefinders are able to compute the distances to obstacles by emitting a laser pulse and measuring the time it takes for the reflected beam to be detected (given that laser light beams move at a known speed). This principle is quite common among sensors, and it accounts for lightweight, low-cost technology [10]. However, it is limited by weather conditions, as laser light might scatter in the presence of clouds, fog, or atmospheric attenuation.

The Light Detection and Ranging (LIDAR) working principle is similar to the laser rangefinder, except it is multi-directional thanks to an oscillatory base; thus, its execution goes beyond simply detecting an obstacle's range, and a 2-D point cloud can be acquired through a vast array of distance and azimuthal measurements pairs. LIDARs installed on UAVs can accurately delineate the shapes of objects at fair distances, (more than 30 m), as demonstrated on a LIDAR-based system for tree measurements [11], thus making them main candidates to incorporate an obstacle detection system.

Radio Detection and Ranging (RADAR) is one of the most popular sensing technologies. It consists of a transmitting antenna that produces electromagnetic waves (in the radio or microwave spectrum) and a receiving antenna, which collects waves echoed from static or dynamic obstacles [12]. Despite being very similar to LIDAR, RADAR technology is distinguished by the frequency of the emitted radiation. The distance between the sensor and the target is also computed by measuring the time lapse between the transmitted and received signal since radio waves also move at a known speed.

Vision technology can acquire richer information from surroundings, involving color and texture, while being cheaper and easier to deploy in comparison to the aforementioned sensors [13]. However, image sensors face challenges in achieving high accuracy due to their dependency on texture, lighting, and weather conditions. Furthermore, all cameras rely on real-time heavy image processing to extract useful information from the chunks of raw data being provided by the sensor [14], thereby greatly increasing the computational complexity of this application. Therefore, vision-based sensors were deemed unsuitable for the present study.

It is important to note that most research in this field focuses on multirotor UAVs. Among these, solutions typically include cameras [15], LIDAR technology [16], or both [17]. That was not the case for the solution presented in [18], where the solution was specifically designed to map indoor spaces with planar structures through graph optimization. Using many 1D lasers to maximize the orientations that are being covered, as opposed to using a single 2-D LIDAR, allows for a more accurate hypothesis of the planar structures—one that is free of assumptions about the horizontal and vertical planes. Furthermore, the viability of an acoustic-based collision avoidance system for a fixed-wing UAV that resorts to microphone data as the main input was also investigated with limited success [19].

Regarding flight planning and collision avoidance, a recent work aimed at implementing UAV path re-planning and evasion maneuvers through deep reinforcement learning [20]. A deep reinforcement learning approach for three-dimensional path planning by using local information and relative distance without global information, i.e., resorting to a partially observable Markov decision process, was proposed [21]. In contrast, the present solution focuses primarily on the detection capacity of different sensors and how to optimize their resources, thus resorting to a simpler Potential Fields collision avoidance method.

Preceding this work, different detection systems were simulated using laser rangefinders and RADARs in different configurations [22]. Through the Potential Fields method and resorting to an optimization algorithm, a possible configuration of a UAV detection system was reached. Subsequently, ultrasonic sensors and laser rangefinders have been employed in the hardware implementation of an effective sense and avoid system on a simple rover [23].

The main goals are to (1) perform a comprehensive study of the four main, active non-cooperative sensor types (ultrasonic sensor, laser rangefinder, RADAR, and LIDAR); (2) develop models for each type and embed them in an obstacle detection and avoidance simulation tool; and (3) perform off-line simulations using randomly generated collision scenarios to obtain optimal multi-sensor configurations in terms of sensor types, positions, and orientations that maximize the obstacle sense and avoidance success rate for a given set of performance parameters of a small fixed-wing UAV.

The current work is limited to 2-D problems, and it is assumed that the UAV is in level flight (constant altitude) at cruise conditions and remains so during the obstacle detection and avoidance stages. For fixed-wing aircraft, this might represent the vast majority of its flight.

2. Sensor Modeling

The next subsections describe the models of active non-cooperative sensors: the ultrasonic sensor, the laser rangefinder, the LIDAR (Light Detection and Ranging) sensor, and the RADAR (Radio Detection and Ranging) sensor. These are illustrated in Figure 2, and are followed by a comparative analysis, as shown in Table 1. Certain models were developed by [24] and are further adapted to the present work.

The relevant sensor specifications are summarized in Table 1. Although the obstacle detection capability depends greatly on the range, field-of-view (FOV), accuracy, and update rate of the sensors, other aspects should also be taken into account during the selection of parts. The size and weight of sensors are crucial factors to consider when designing a S&A system for small UAVs since it may be counterproductive to add detection capability at the cost of reduced vehicle maneuverability. This is likely not the case for the particular

set of sensors in this study, with the MB1242 sonar being the smallest and lightest; followed by the slightly larger and heavier LW20/C laser; then the SF45/B LIDAR that is almost double in size; and the US-D1 RADAR, which—while the largest and heaviest—is still sufficiently compact for application in small UAVs. Power consumption can be particularly important since most UAVs are battery powered; thus, LIDAR and RADAR are at a clear disadvantage compared to the ultrasonic sensor. Regarding acquisition cost, the ultrasonic sensor is the cheapest sensor, while the laser-based and RADAR sensors are considerably more expensive. Unexpectedly, the SF45/B LIDAR with a variable FOV is more costly than the LW20/C one-dimensional laser rangefinder, and the US-D1 RADAR is the most expensive at twice the cost of the laser due to its pricier technology.

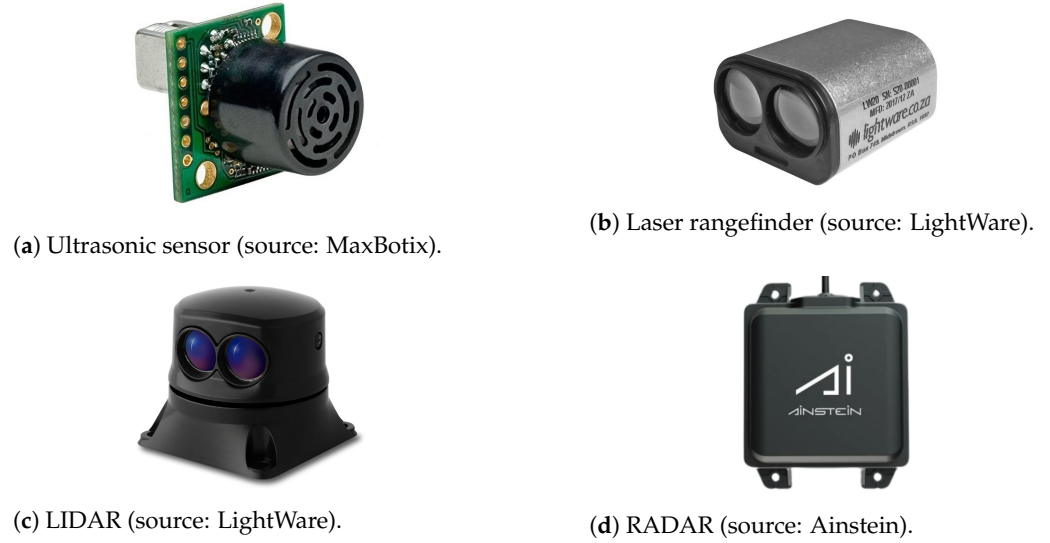


Figure 2. Active non-cooperative sensors.

Table 1. Sensor hardware specifications.

	Ultrasonic Sensor MB1242 [25]	Laser Rangefinder LW20/C [26]	LIDAR SF45/B [27]	RADAR US-D1 [28]
Range (m)	7	100	45	50
Horizontal FOV (°)	0	0.3	20–320	43
Resolution (cm)	1	1	1	–
Accuracy (m)	0.1	0.1	0.1	0.04
Update rate (Hz)	7	388	5000	100
Power supply voltage (V)	3–5.5	4.5–5.5	4.5–5.5	5–5.5
Power supply current (mA)	4.4	100	300	400
Outputs and interfaces	Serial and I2C	Serial and I2C	Serial and I2C, Micro USB	UART, CAN
Dimensions (mm)	22 × 19 × 15	30 × 20 × 43	51 × 48 × 44	108 × 79 × 20
Weight (g)	5.9	20	59	110
MSRP (€)	40	300	450	600

2.1. Ultrasonic Sensor

This type of sensor has a wide FOV that translates to a beam pattern with axial symmetry, as represented in Figure 3.

Since the ultrasonic sensor only outputs a distance, it leaves all the interior beam points located at a specific distance from the UAV as potential object positions. This results in errors that can be avoided, as well as other issues that arise from sound reflection. The

sound reflection law states that the reflected sound wave's angle with the normal of the surface is preserved. Thus, the ultrasonic sensor requires a perpendicular surface in order to detect an object, which, in turn, implies that the targets format is crucial to the mission's success. It is vital to recognize that the final results can only be used as a reference given that these simulations only use spherical shape targets (and different target formats could either improve or worsen the outcome). In short, the model must check for the following possibilities at all times:

1. The presence of any spherical surface point within the sonar beam pattern;
2. The perpendicularity of the sound wave direction with its reflecting surface.

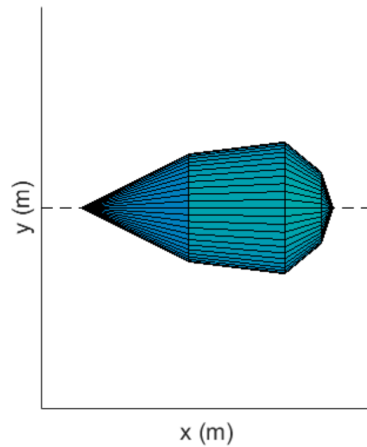


Figure 3. Ultrasonic sensor beam pattern [23].

Verifying these conditions requires considerable computing time. Therefore, a progressively complex approach was implemented [23]. First, the beam pattern is reduced to a cylinder. When the center of the obstacle is found to be inside the cylinder, a more thorough analysis is performed to identify which portion of the spherical surface, if any, is in fact inside the beam pattern. The last stage addresses the perpendicularity issue. The final surface computed in the preceding phase is defined as a list of points. The aim is to calculate the angle between the direction of the sound wave and the tangent surface of the sphere at that precise location. The point is deemed to have been picked up by the sonar if the angle is close to 180° (with a 5° tolerance). Although the vast majority of the final surface points were inside the beam pattern, all of the points that were designated as detectable required a second examination. The closest point to the UAV position (among those that passed these filters) was chosen as the detected point. The UAV reference point, which will serve as the reflection point for the trajectory re-planning algorithm, will be situated on the beam pattern axis at the same distance from the UAV as the detected point.

2.2. Laser Rangefinder

Considering the obstacles as spheres, the reflection point can be modeled as a simple interception between a line and a spherical surface in Figure 4, which is given by

$$\|\mathbf{x} - \mathbf{c}\|^2 = r^2, \quad (1)$$

$$\mathbf{x} = \mathbf{o} + d\hat{\mathbf{u}}, \quad (2)$$

where \mathbf{x} is the detection point on the line and/or sphere, \mathbf{c} is the center point of the sphere, r is its radius, $\hat{\mathbf{u}}$ is the unit vector that defines the line direction in 3D space, and d is the distance from the origin of the line \mathbf{o} . Combining both equations leads to an easily solvable quadratic equation,

$$d^2(\hat{\mathbf{u}} \cdot \hat{\mathbf{u}}) + 2d[\hat{\mathbf{u}} \cdot (\mathbf{o} - \mathbf{c})] + (\mathbf{o} - \mathbf{c}) \cdot (\mathbf{o} - \mathbf{c}) - r^2 = 0, \quad (3)$$

which returns a solution d if $0 < d < R_d$, where R_d is the sensor detection range. In real conditions, the laser would not reach the furthest point, it would instead reflect on the closest one. Therefore, if there are two solutions in this interval, only the smallest one prevails. The reflection point with a spherical surface can be easily obtained from Equation (2).

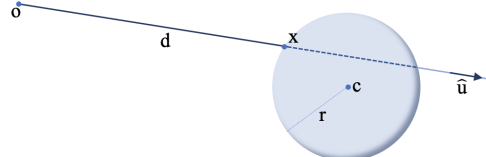


Figure 4. Laser rangefinder detection model.

2.3. LIDAR

This type of sensor is not limited to a distance output as it can also provide the system with an azimuthal angle where the distance was measured, i.e., the LIDAR model has to account for outputs with polar coordinates. The LIDAR model is very similar to the laser rangefinder's, in which it makes only the points that are closest to the sensor detectable. This implies that if an object is completely visible, then only half is detected, and the remaining half of the obstacle is reconstructed via symmetry, where the center of symmetry is the medium point of the segment connecting the first and last point of the cluster. In the present simulations, this distance corresponds to the diameter of the obstacle. The symmetry assumption brings no drawbacks since the LIDAR is continuously scanning and updating the detected points, thus providing an up-to-date front-facing geometry of the obstacle. The model discards obstacles that are hidden or outside the field of view (FOV).

A common issue lies within higher distances between consecutive points in farther obstacles, which results in smaller detected dimensions (compare Obstacle and Obstacle Model in Figure 5). To solve this problem, the measured diameter is passed through the time filter, as proposed in [29],

$$D_k = D_{k-1} + G(D_m - D_{k-1}), \quad (4)$$

where $G(0 < G < 1)$ is the filter gain, D_k is the filtered diameter at instant t_k , D_{k-1} is the filtered diameter at instant t_{k-1} , and D_m is the measured dimension at instant t_k . The gain must be carefully chosen because it affects how quickly the dimensions change. While a small gain (i.e., a slow variation) is better for noisy surroundings, it is not appropriate for objects with high relative speeds. The gain is given by

$$G = 1 - \sqrt[n]{1 - p}, \quad (5)$$

where p corresponds to a fraction that represents the desired accuracy of the dimensions and n corresponds to the number of filter cycles required to get an accuracy of p . Classic Kalman filters [30] were employed for the tracking phase, where the motion of obstacles was assumed to be two-dimensional, linear, and constant over successive scans. This simplification, which takes into account a high scanning frequency, accurately captures the targets' state.

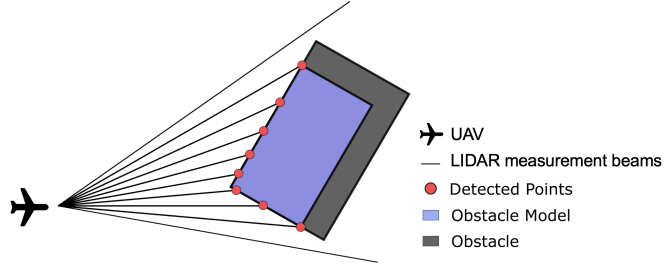


Figure 5. Obstacle reconstruction using a LIDAR (adapted from [24]).

The LIDAR model in use (based on the LightWare's SF45/B) has a specific update rate, but it is possible to set its angular velocity (scanning speed) up to a maximum of 6.3 rad/s. However, by choosing faster sweep speeds, the arc of circle that is not being detected between each measurement increases, thus increasing the likelihood of missing an obstacle smaller than that arc. This effect is illustrated in Figure 6, where the length of the arc traversed Δs varies analytically with the distance to the sensor and the angular velocity. At maximum scanning speed (ω_{max}), this 45 m range LIDAR might not detect obstacles that are smaller than 8 m wide at this distance. However, if covering a larger area quickly is more important, sacrificing some visibility at the maximum range might be acceptable. Ultimately, the compromise should be based on the specific needs and constraints of the system.

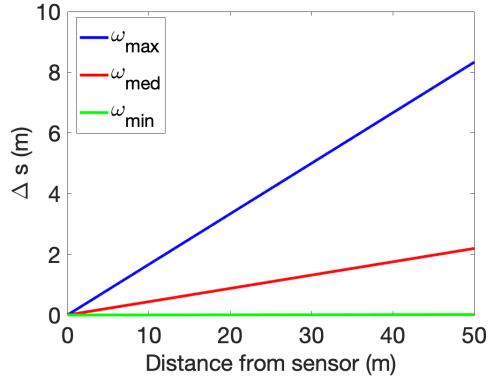


Figure 6. SF45/B undetectable arcs for different scanning speeds.

2.4. RADAR

In this case, the state estimation is more complex than the one employed in the LIDAR model (given the RADAR sensor provides the distance, azimuth, and elevation of the observed obstacles). These outputs are spherical, but only the polar components (distance and azimuth) are considered in the 2-D model. Since the intruder dynamics are best described in rectangular coordinates, the converted measurement Kalman filter (CMKF) was used to convert the measurement data in polar coordinates into a Cartesian coordinate system, so that the tracking could be realized through a linear Kalman filter [31]. The 2-D model used in the simulations was then represented by

$$\begin{cases} x_m^u &= \lambda_\alpha^{-1} r_m \cos(\alpha_m) \\ y_m^u &= \lambda_\alpha^{-1} r_m \sin(\alpha_m) \end{cases}, \quad (6)$$

where (x_m^u, y_m^u) are the measurements converted to the Cartesian frame, r_m is the measured range, α_m is the measured azimuth, and λ_α is the bias compensation factor expressed as

$$\lambda_\alpha = e^{-\sigma_\alpha^2/2}, \quad (7)$$

where σ_α is the standard deviation of the noise in the azimuth measurements. The compensation of the bias is multiplicative due to the use of the unbiased conversion and modeling the measurement errors as Gaussian white noise. The covariance matrix used in the Kalman Filter is given by

$$\mathbf{R}_u = \begin{bmatrix} \text{var}(x_m^u \mid r_m, \alpha_m) & \text{cov}(x_m^u, y_m^u \mid r_m, \alpha_m) \\ \text{cov}(x_m^u, y_m^u \mid r_m, \alpha_m) & \text{var}(y_m^u \mid r_m, \alpha_m) \end{bmatrix}, \quad (8)$$

with the details of the computation of these variances found in [32].

2.5. Multi-Sensor Data Fusion

All of these sensors (and respective models) provide inputs that allow the avoidance system to actuate. However, if the system's architecture is composed by more than one sensor, the data provided must be merged in some way. The sensor models previously described provide the required mutual transformation of their measurements into one global Cartesian coordinate system. Also, synchronization is guaranteed by the time schedule used for retrieving the obstacle sensing data from models.

Following the best practices proposed in a similar application [33], the weighted filter method was used in the present study for data fusion. The principle behind this method is simple: each sensor is given a weight that is based on how reliable it is. Reference data sensors that provide information about the UAV state must be installed. Considering that changes in the distance to obstacles correspond to changes in the UAV location, reference data sensors like IMUs and optical flow sensors are used to assess the accuracy of the main data and aid in selecting the best sensor. In the particular case of fixed obstacles, the aforementioned variances in distance ought to match. The weights are then calculated by applying a differential norm to compare all of the conceivable sensor combinations of the main data and reference data. In each instant, the obstacle distance measurement corresponding to the sensor with the lowest weight is chosen, and the remaining measurements are discarded on the grounds that they are corrupted. Nonetheless, the sensor readings are fused in accordance with their weights if the computed weights have a low variation.

3. Collision Avoidance

Following previous works [22,24], the Potential Fields method was chosen to solve the local path planning problem. A brief explanation of the algorithm and its implementation in the simulation tool are described next.

3.1. Potential Fields Method

Based on Coulombs law, the Potential Fields method conceptualizes waypoints and obstacles as oppositely charged particles. It translates the pre-determined UAV flight path to the waypoints charged with an attractive potential, while the detected obstacles become charged with a repulsive potential. Upon the successful implementation of this collision avoidance method, the simulated UAV tries to avoid obstacles by trajectory re-planning.

Each obstacle is modeled as a circle with various safety zones, which serve pivotal roles in both collision detection and avoidance simulations, as seen in Figure 7. The collision radius R_c circumscribes the obstacle size, triggering a collision event if the UAV violates this radius. The safety radius R_s specifies the minimum separation distance between the UAV and the obstacle, accounting for deviations and uncertainties during detection and avoidance stages, which trigger a close call event if breached. The detection radius R_d represents the sensor detection range.

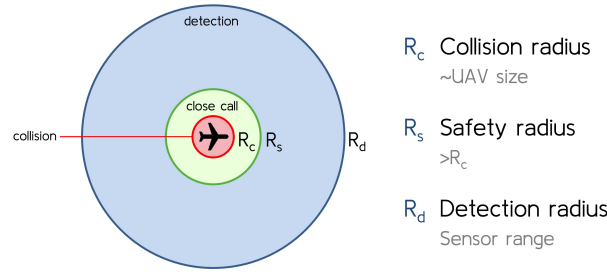


Figure 7. Safety zone radii.

For each potential collision scenario (see its generation in Section 4.1), there are three possible outcomes of the avoidance maneuver, as represented in Figure 8, based on the radii breach: success, close call, and failure.

3.2. Implementation in Simulation Tools

By gathering the obstacle distances from the onboard sensors from the obstacle detection stage (according to Section 2.5), an obstacle screening process was run. A list of obstacles was strategically organized based on the urgency of the detected collision possibilities, thereby assuming the straight projection method, i.e., the current state of the obstacle is projected into the future along a straight trajectory that is made at a constant velocity. An evasive maneuver will be triggered if the minimum distance between the UAV and an obstacle is smaller than the safety radius.

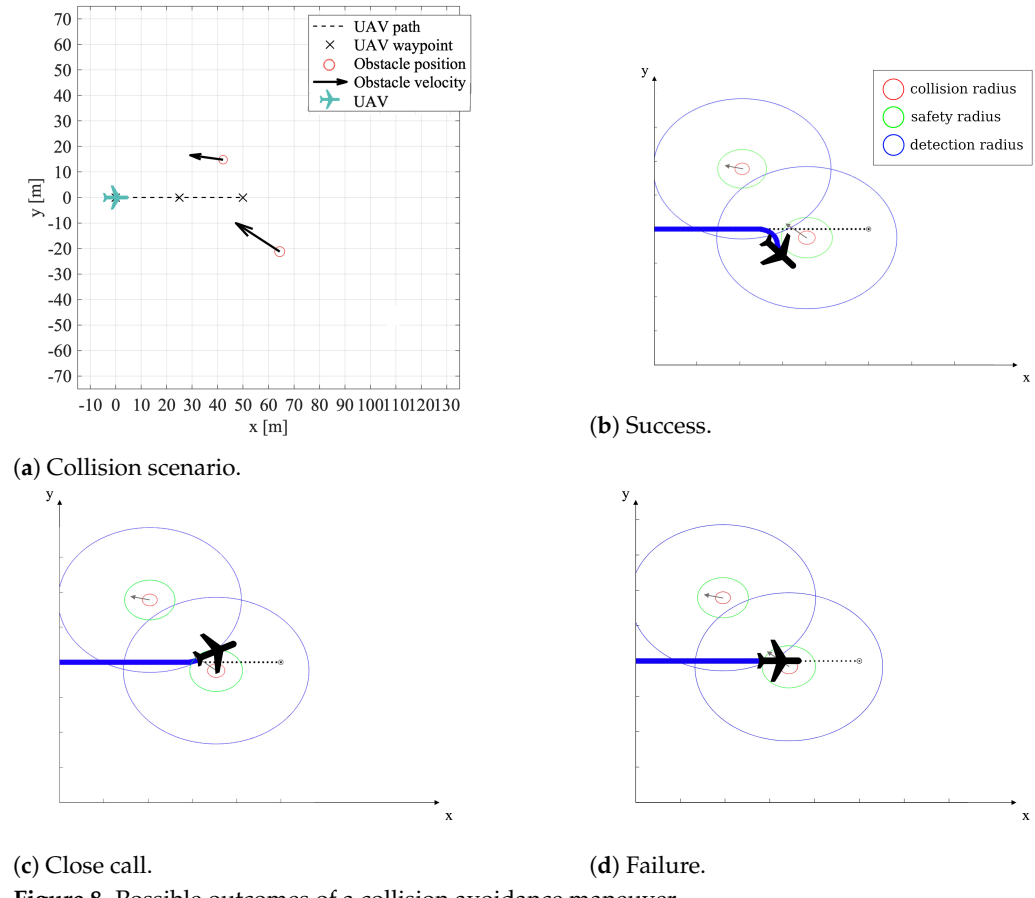


Figure 8. Possible outcomes of a collision avoidance maneuver.

Mathematically, the collision detection method consists of computing the closest point of approach (CPA) between the UAV and the obstacle, and it is assumed that both vehicles will maintain constant velocities. Then, the motion of two vehicles, A and B, are described

as $A(t) = A_0 + \mathbf{v}_A t$ and $B(t) = B_0 + \mathbf{v}_B t$, and the distance between them at an instant t is given by $\|A(t) - B(t)\|$. By solving its derivative, the instant corresponding to the minimum distance between the two points (t_{CPA}) is given by

$$t_{CPA} = \frac{-(A_0 - B_0) \cdot (\mathbf{v}_A - \mathbf{v}_B)}{\|\mathbf{v}_A - \mathbf{v}_B\|^2}. \quad (9)$$

Through knowing the value of t_{CPA} , the minimum distance between the two vehicles can be easily computed as

$$d_{CPA} = \|A(t_{CPA}) - B(t_{CPA})\|. \quad (10)$$

To overcome linear projection simplification, these computations are regularly repeated to account for other possible UAVs and moving obstacle maneuvers. In the case of multiple collisions being detected, the obstacles are sorted by the ascending order of their t_{CPA} .

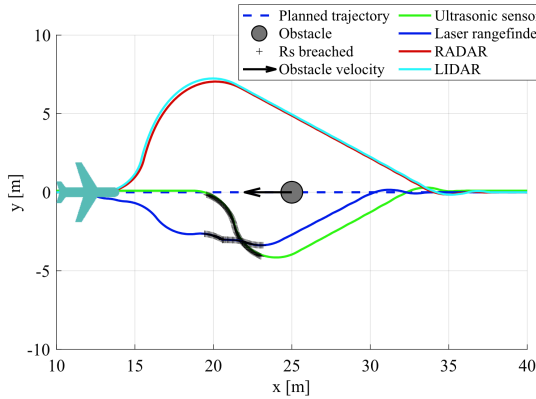
Upon detecting a potential collision, an avoidance strategy is implemented to maintain a safe separation between the UAV and the identified obstacles. To accomplish this, iterative local paths are generated until there are no longer any obstacles representing potential collision risks. If waypoints are found to be blocked by obstacles and have become unattainable, they are discarded in this re-planning stage.

As for the path re-planning strategy, since UAVs must always give way to manned aircraft (and as the sensing is assumed to be non-cooperative), the UAV will always make an evasive maneuver while respecting the Rules of the Air [34]. In the case of an imminent collision, the avoidance strategy is as follows: (i) the UAV turns right if the intruder is in a head-on collision path or to the right of the UAV; (ii) the UAV turns left if the intruder is approaching from the left; and (iii) in the case of a static obstacle, the direction in which the obstacle is circled around is the one that corresponds to the smaller path to reach the goal. Climb and descent rules do not need to be taken into consideration as this work only presents a 2-D level flight simulation. In the current version, the UAV response is based solely on the system dynamics, which is limited by its maximum turning rate without any legislative restrictions being considered. More details about the implemented avoidance algorithm can be found in [35].

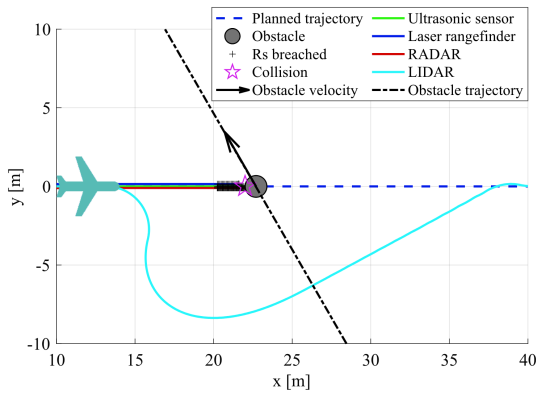
3.3. The Benchmark of Sensor Performance

Prior to any optimization, the response of the UAV to imminent collisions was studied to compare the performance of each sensor type. The UAV was set traveling at 8 m/s and equipped with a single sensor pointing forward. First, the UAV was set on a head-on collision course with an obstacle at an incoming speed of 10 m/s with a radius of 2 m and a safety radius of 4 m. The resulting collision avoidance trajectories are shown in Figure 9a. Although the obstacle is always properly tracked and avoided, the re-planning maneuvers differ. When equipped with a ultrasonic sensor, the UAV was already inside the obstacle action radius when detection occurred, so it could not avoid breaching the safety radius (close call). When equipped with a laser rangefinder, the UAV reacted the earliest and slightly changed its direction but, as a result of the obstacle stopping being tracked due to the sensor having an almost null FOV, the safety radius ended up also being breached. As for the RADAR and LIDAR sensors, the corresponding evasion maneuvers started approximately at the same point due to their similar range, and this resulted in a successful evasion.

A similar test was made with the UAV set on a 60° angled collision course with an obstacle moving at a speed of 12 m/sm, as represented in Figure 9b. In this case, only the LIDAR sensor was able to properly track and execute the evasion maneuver, without ever breaching the safety radius, in a timely manner. All other sensors were unable to track the obstacle in a timely manner due to their reduced range or FOV, thus leading to a collision.



(a) A head-on collision.



(b) A 60° angled collision.

Figure 9. UAV collision avoidance response to obstacle detection when equipped with different sensors.

4. Optimal Sensing System

An optimization study was conducted to find the types of sensors and respective orientations relative to the UAV longitudinal axis that result in the best collision avoidance performance. To do so, a set of randomly generated collision scenarios with both fixed and moving obstacles were generated. The sensors modeled in Section 2 were tested for each of these scenarios, and their orientations were varied until optimal configurations were found.

4.1. Scenario Generation

To create scenarios suitable for this study, a scenario generation algorithm was used, in which the predetermined path and waypoints of the UAV as an input was accepted before combining them with a list of moving and static obstacles to produce a scenario [23]. Each scenario must specify the obstacle's initial position, velocity, and radius. It should also include a pre-planned path and waypoints that the UAV must follow.

Different bounds were defined regarding the kinematic and dimensional properties of the obstacles and the UAV itself. Various stochastic and partially stochastic processes were then extracted from these intervals, creating random values for the different variables, as depicted in Figure 10. Partially stochastic processes were used in two different cases: determining the velocity orientation of moving obstacles and setting the position of static obstacles. In the former, the goal was to ensure that, initially, the direction of the obstacle's velocity should point to the center of the domain rather than pointing outward, thus increasing the possibility of collision. In the latter, the position of any static obstacle must not be within a determined safety radius around the waypoint given that the UAV must pass through it. All remaining bounds but one were used to select a completely random value that ultimately defined each set of obstacles. In addition, a pre-determined flight path was loaded, which accounted for a non-stochastic process, into each scenario.

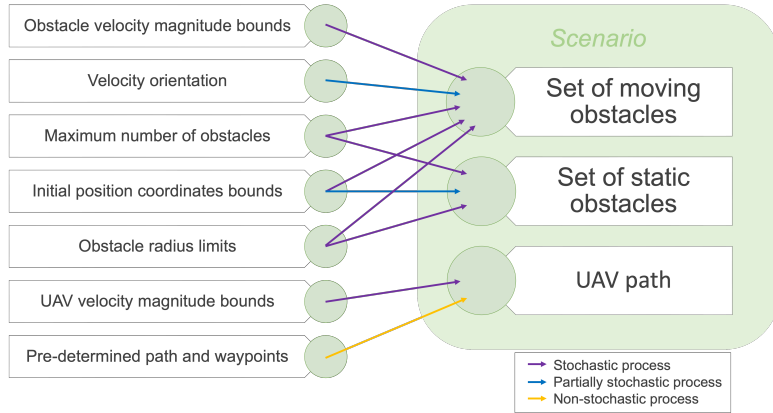


Figure 10. Scenario generation algorithm [23].

Finally, each scenario was tested for potential collisions using a flight simulator without any sensors (with the obstacle avoidance strategy turned off). This was then discarded if the UAV did not go beyond any obstacle's safety radius R_s throughout the whole flight simulation. This function was repeated until n scenarios with an impending collision were generated.

In this study, forty collision-leading scenarios were randomly generated, with obstacle parameters varying according to the limits set in Table 2 for the UAV speed, number, and size of fixed and moving obstacles, as well the velocity of the latter. The UAV speed and maneuvering capabilities were based on the Tekever AR4 small fixed-wing model, in which a maximum turning rate of $45^\circ/\text{s}$ [36] was assumed.

An example of a resulting collision scenario is plotted in Figure 11, where two moving obstacles in a collision course with the planned UAV flight path can be observed.

Table 2. Data for the randomly generated collision scenarios.

UAV Speed	Number of Fixed Obstacles	Number of Moving Obstacles	Obstacle Radius	Obstacle Speed	Obstacle Direction
[5, 15] m/s	{0, 1, 2}	{0, 1, 2}	[0.5, 2] m	[5, 15] m/s	[0, 90]°

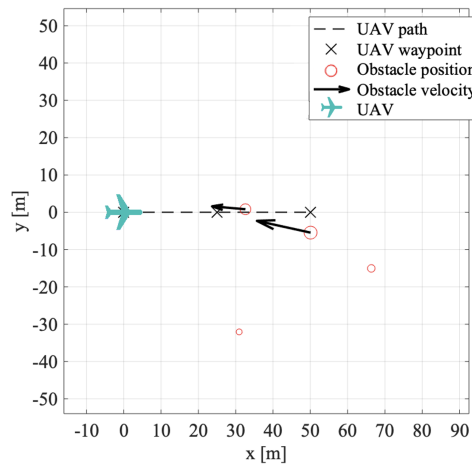


Figure 11. Randomly generated collision scenario.

4.2. Optimization Technique and Problem Formulation

To determine the optimal sensor configuration, different sensor sets were tested. The parameters that characterize each sensor model were obtained from their technical manuals

or inferred from the available data summarized in Table 1. Since our simulations were restricted to the horizontal plane of motion, the vertical FOV was not relevant.

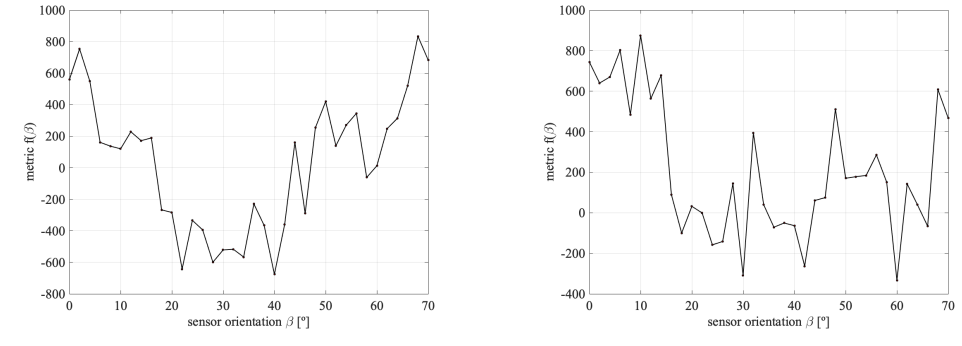
Given that all sensors may be mounted at an angle β relative to the UAV longitudinal axis, our model assumed the use of two symmetrical sensors at the angles β and $-\beta$ whenever $\beta \neq 0$.

In order to optimize the sensor orientation β , a Sense and Avoidance (S&A) metric function $f(\beta)$ was minimized and defined as

$$f(\beta) = \sum_j \sum_i \left(-d_{\min}(i) + \phi_1 |\max(R_s(i) - d_{\min}(i), 0)|^2 + \phi_2 |\max(R_c(i) - d_{\min}(i), 0)|^2 \right), \quad (11)$$

where the first term drives the evasion maneuver to maximize the minimum distance d_{\min} between the UAV and the obstacle i , the second term represents the penalty when the minimum distance violates the safety radius R_s ($d_{\min} \leq R_s$), and the last term represents the penalty when the minimum distance violates the obstacle collision radius R_c ($d_{\min} \leq R_c$). The metric accumulates not only for every obstacle i in each scenario, but also for all scenarios j . In order to penalize collision cases more than close calls, the weights were set to $\phi_1 = 10$ and $\phi_2 = 50$. Notice that the sensor orientation β was kept fixed during the simulations with the 40 scenarios, and it was only considered variable when determining the best installation orientation of the sensor attached to the aircraft (Equation (12)).

The deceptive look of the metric function defined in Equation (11), might suggest that least-squares or quadratic programming methods would be adequate. However, the metric is far from satisfying the required properties since the terms $d_{\min}(i)$ vary in a highly non-linear fashion with variable β . Figure 12 shows the metric function value defined in Equation (11) for two particular sensor sets: (i) using only a pair of laser rangefinders with a 100 m range that symmetrically pointing forward with an angle β with respect to the UAV longitudinal axis; and (ii) adding a RADAR with a 120 m range pointing in the direction of the UAV longitudinal axis. In both cases, the metric function $f(\beta)$ proved to be multimodal and noisy.



(a) A pair of laser rangefinders. (b) A pair of laser rangefinders and one RADAR.
Figure 12. S&A metric as a function of laser rangefinder orientation.

These identified metric function properties conditioned the choice of the optimizer. Gradient-based optimization methods were discarded since they would struggle in the presence of noise and would become stuck in local minima. Among the vast choice of gradient-free (or derivative-free) methods available in the literature [37], in particular those that find near-global solutions for non-convex problems, the Genetic Algorithm (GA) implemented in MATLAB was selected in this work. While there are other newer and better performing methods, its ease of implementation prevailed when making the choice. Its higher computational cost is acceptable since its usage occurs in the design stage of the obstacle detection system, i.e., prior to the installation of the sensors and pre-flight. The stochastic nature of GA, as it involves crossover (exploitation) and mutation (exploration) operators over a population of solutions, allows for it to explore a broader solution space and adapt to the challenges posed by noise and multimodality, as well as allows for it to

handle the uncertainty introduced by noisy objective functions more effectively. Additionally, the exploration-exploitation balance in the GA enables it to navigate multimodal landscapes by maintaining a diverse population and evolving solutions over generations (iterations).

The problem can be posed as a non-linear-bound-constrained optimization,

$$\begin{aligned} & \text{minimize } f(\beta) \\ & \text{w.r.t. } \beta \\ & \text{subject to } \beta_{\min} \leq \beta \leq \beta_{\max} \end{aligned} \quad (12)$$

where β_{\min} and β_{\max} are the lower and upper bounds of β , respectively, to be defined for each particular case. Notice that β is a vector if multiple sensors are used.

The initial GA population was set to be created with a uniform distribution. The crossover function was set to create 80% of the population in each generation. Moreover, because the variables were bounded, the mutation function randomly generated directions that were adaptive with respect to the last successful or unsuccessful generation, where the chosen direction and step length satisfied the set bounds. The convergence criteria were set such that the global minimum was found in a timely but accurate manner: a function convergence of 10^{-3} was used with 10 stall generations, and a maximum of 50 generations were prescribed. The population size was set to 30 individuals. These parameters were chosen following best practices. Larger populations and stricter convergence criteria were also tested but led to no significant impact on the results presented. The simulations were run on an 1.4 GHz Intel quad-core i5 with 8 GB 2133 MHz RAM.

4.3. Optimal Sensing Configurations

The following subsections are dedicated to detailing the proposed sensing architectures, in which further explanations of each solution and the respective optimal results are detailed. In the end, the performance of the different sensor sets are summarized and compared in order to implement the best solutions.

4.3.1. Two Ultrasonic Sensors

For a set of two ultrasonic sensors, the orientation of each sensor was bounded between 0° and 90° from the longitudinal axis, and the range was set to 6 m. To simplify the problem, the two sonars were considered to have a symmetrical orientation, resulting in just one design variable. A narrow beam pattern was adopted to reduce computational cost.

The GA minimization terminated after 20 iterations due to average changes in the fitness value being less than the specified tolerance. It performed 592 function evaluations in 18 h and 36 min, and it reached an optimal orientation of 36.5° (see Figure 13).

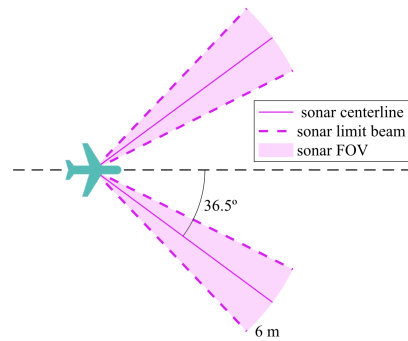


Figure 13. Optimal orientation for two ultrasonic sensor configurations.

The results, summarized in the second line of Table 3, were far from satisfactory since the safety radius was breached many times, thus leading to a collision rate of 10 %. Compared to a single sonar pointing forward (see first line in Table 3), a pair of sonars

brought little to no gains in the detection performance for the type of UAV under study. This was expected due to the short range of ultrasonic sensors, which makes it impossible for the UAV to detect the obstacle, re-plan its trajectory, and perform the avoidance maneuver in a timely manner.

When considering a UAV traveling at maximum speed (15 m/s), the ultrasonic range (6 m) was traversed in 0.4 s. In the worst case with an obstacle moving at 15 m/s head on, the available reaction time of just 0.2 s was clearly insufficient.

4.3.2. Two Laser Rangefinders

Analogous to the previous case, a set of two laser rangefinders with symmetrical orientations but with a sensing range of 100 m was considered.

After 19 generations, the GA optimization algorithm finished having completed 564 function evaluations in a computing time of 1 h 25 min. The optimal sensor orientation was 34.4° , which corresponds well with one of the approximate minimums shown in the preliminary study, as shown in Figure 12. The optimal two laser rangefinder sensor configuration is illustrated Figure 14.

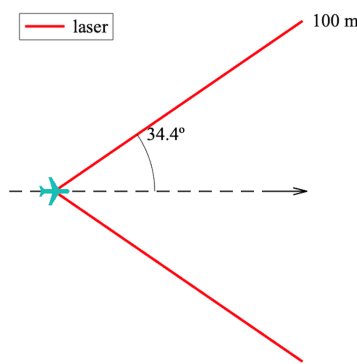


Figure 14. Optimal orientation for a two-laser rangefinder configuration.

The performance of this optimal configuration is summarized in the fourth line of Table 3. Although the optimal configuration only failed once in 40 scenarios, the safety radius was breached in 23 of them. This result was expected since a UAV equipped only with two laser rangefinders (with extremely narrow FOVs) is not capable of properly tracking moving obstacles when collisions are imminent. Also, there were gains when using more than one laser (see third line of Table 3), which made up for the reduced, almost zero, individual FOVs.

Compared to the previous case of ultrasonic sensors, these simulations demonstrated that laser rangefinders not only prevent more collisions, but also more close calls. This is mainly a consequence of their large detection range advantage (100 m), which prevail over their almost zero FOV. Overall, these sensors perform better under the given circumstances.

When considering a UAV traveling at 15 m/s, the laser range was traversed in 6.7 s. If an obstacle was also moving at 15 m/s head on, the available reaction time was 3.3 s, so it was typically enough to track an obstacle and re-route, provided it was tracked because of a reduced FOV.

4.3.3. Two RADARs

Once again, the two RADAR sensors were considered to be symmetrical on the UAV longitudinal axis and the orientation spanned from 0° to 90° . Each RADAR had a range of 50 m, an accuracy of 0.04 m, and a FOV of 43° .

After 11 generations, the optimizer finished 340 function evaluations and a computing time of 1 h 11 min. The optimal RADAR orientation was 9.2° , as illustrated in Figure 15.

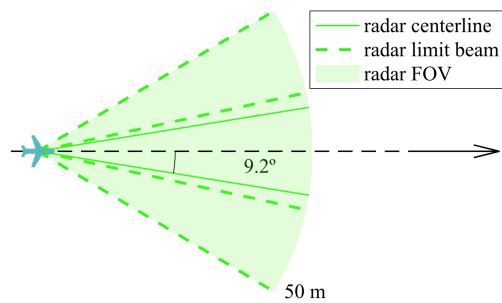


Figure 15. Optimal orientation for a two-RADAR configuration.

Another configuration worth studying would be a sensor orientation that is close to 21.5° , which would yield the same result as if the UAV were equipped with a single RADAR with a double FOV (86°). Table 3 includes a comparison of a single RADAR pointing forward and a solution with two RADARS in the seventh to eighth lines.

Regarding actual collisions, obstacles that approach the UAV from an angle are more likely to be detected by the optimal solution rather than by the single-RADAR configuration. As can be seen in Table 3, the number of failures increased as the orientation decreased (for this particular case), which in turn made the success rate decrease.

By overlapping the FOV of the two sensors, the accuracy was reduced through the data fusion algorithm. Thus, in this case, having a narrower FOV ($\beta = 9.2^\circ$) and, in turn, the juxtaposition of both RADARs proved to be almost as effective as the double FOV configuration ($\beta = 21.5^\circ$).

These simulations showed that the accuracy of RADAR proved to be impactful on the precision of obstacle tracking compared to that of the laser sensors. The latter's accuracy can not be reduced through the data fusion algorithm since a laser FOV would not overlap (0°). Despite having a broader FOV and resulting in less close calls, the RADAR solution led to just as many collisions, which means that the two-laser rangefinder configuration displayed the same success rate. It is reasonable to say that, while RADAR FOVs are more crucial for detecting obstacles, the sensor's accuracy is the most significant factor for effective collision avoidance.

When considering a UAV traveling at 15 m/s, the RADAR range (50 m) was traversed in 3.3 s. If an obstacle was moving at 15 m/s head on, the available reaction time was 1.7 s, which might be a challenging time to successfully complete an evasion maneuver. However, the tracking is likely to be more successful given the large FOV.

4.3.4. Two LIDARs

Each LIDAR was modeled with a range of 45 m, an accuracy of 0.1 m, and a variable FOV. According to hardware specifications (see Table 1), this FOV can range from 20° to 320° ; thus, a FOV of 180° was chosen. This value ensures a reasonable trade-off between timely scanning frequency and a broad scope.

However, this makes optimization redundant due to the nature of the scenario generation algorithm used: because the obstacles spawn inside the limits of the scenario, it is worthless to track the area behind the UAV in the initial instant. Furthermore, from this instant on, if an obstacle was positioned behind the UAV, it would have already been tracked before due to the wide FOV and long range of the LIDAR. The overlapping of the FOV in the case of a two-LIDAR solution did not prove to be advantageous either. (Note that this was only verified for a FOV of 180°). The problem would only arise if a narrow FOV was set due to measurement speed considerations (see Section 2.3). For a smaller FOV, it would be convenient to optimize the sensor orientation.

In this particular case, it is fair to state that the most beneficial solution would be to use a single LIDAR pointing forward since it decreases hardware cost. This configuration is illustrated in Figure 16.

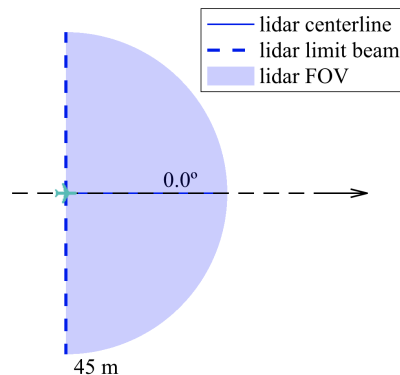


Figure 16. Single-LIDAR configuration.

The last line of Table 3 includes the performance of the single-LIDAR configuration. Compared to the previous types of sensors studied, the LIDAR performed better overall. The reasonable detection range and the wide FOV reduces the chances of close calls and eliminates the possibility of failure.

When considering a UAV traveling at 15 m/s, the LIDAR range (45 m) was traversed in 3 s. If an obstacle is moving at 15 m/s head on, the available reaction time is 1.5 s, so a similar obstacle detection and avoidance performance to the RADAR is expected.

4.4. Performance Comparison of Sensor Sets

Other solutions that involved three sensors were optimized; for example, two laser rangefinders that were symmetrical about the UAV longitudinal axis and whose orientations were bonded between 0° and 70°, and one fixed RADAR pointing forward. This configuration was also replicated with two lasers and one LIDAR; two RADARs and one laser; and two RADARs and one LIDAR. The performance of the optimal version of these sets of sensors, as well as the results from the solutions with only one type of sensor that are discussed in the previous subsections, is summarized in Table 3. Optimizations with different sets of sensors were performed but left out of this table in order to avoid redundancy in the results.

Table 3. Comparison of the optimal performance for the different sensor sets studied.

Sensor Configuration Set	Metric $f(\beta)$	Failure	Close Call	Success Rate
1 SONAR @ 0°	1203.8	4/40	32/40	87.5%
2 SONARs @ 36.5°	804.0	4/40	30/40	90.0%
1 laser @ 0°	111.1	2/40	28/40	95.0%
2 lasers @ 34.4°	-414.0	1/40	23/40	97.5%
2 lasers @ 63.4° + 1 RADAR @ 0°	-1240.4	0/40	11/40	100.0%
2 lasers @ 10.0° + 1 LIDAR @ 0°	-1606.4	0/40	8/40	100.0%
1 RADAR @ 0°	-312.3	4/40	13/40	90.0%
2 RADARs @ 9.2°	-1171.0	1/40	12/40	97.5%
2 RADARs @ 21.5°	-1141.7	1/40	12/40	97.5%
2 RADARs @ 35.3° + 1 laser @ 0°	-1480.1	0/40	9/40	100.0%
2 RADARs @ 28.1° + 1 LIDAR @ 0°	-1574.3	0/40	9/40	100.0%
1 LIDAR @ 0°	-1480.1	0/40	9/40	100.0%

As seen before, for the set of scenarios tested, RADAR performed better than the laser rangefinder, which, in turn, performed better than the ultrasonic sensor if only one sensor type was to be used. Nonetheless, this is tightly dependent on the sensor characteristics, such as range, FOV, and accuracy. Furthermore, a single LIDAR was enough to outperform all other types of sensors.

As expected, all the solutions that present a 100% success rate include either a RADAR or a LIDAR in their configuration, thus attesting the importance of sensor range and FOV

for a timely trigger of the avoidance maneuver. If the LIDAR is kept out, it is the two-RADAR and one-laser rangefinder solution represented in Figure 17a that produced the least collisions and led to the least close calls. From these findings, and because of the 0° FOV of a laser rangefinder, it is expected that increasing the number of sensors even more would lead to an even better performance, though at a higher hardware cost.

When comparing the solutions that include a LIDAR, it was proved that it is not significantly advantageous to pair it with other types of sensors since it already performs distinctively well on its own. The single-LIDAR solution, as shown in Figure 17d, exhibited a 100% success rate. This meant that no collisions were registered due to its wide FOV and considerable range, thus making it able to detect obstacles before they become a threat without the aid of additional sensors. Regardless, the two-laser (Figure 17b) and the two-RADAR (Figure 17c) solutions were beneficial for also reducing the likelihood of close calls. Despite the LIDAR configuration having a wide FOV that was not increased by either configuration, the chances of breaching the safety radius decreased because the other sensors provided additional detection capacity, i.e., since the LIDAR swept the designated area at a certain frequency, there were time instants when a fraction of the area within the LIDAR FOV was 'unsupervised'. Therefore, it is useful to have another set of sensors that track obstacles approaching from that specific area.

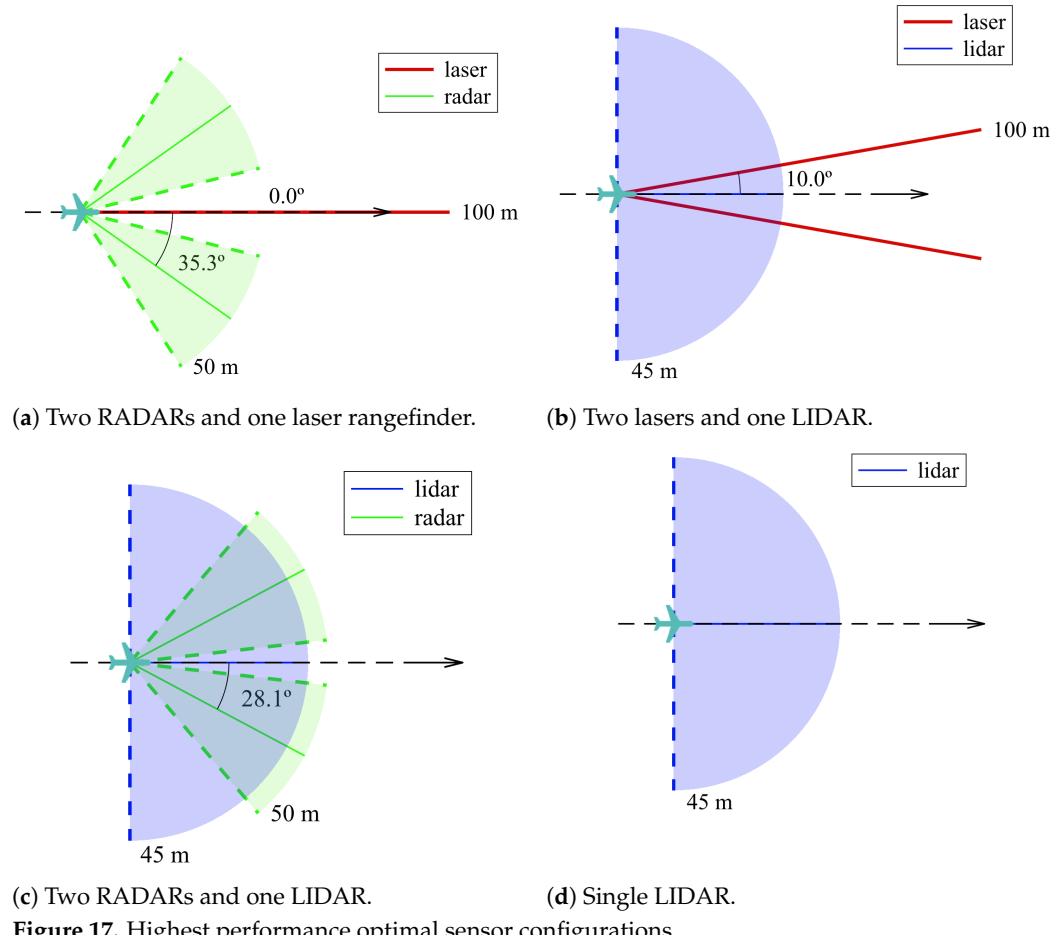


Figure 17. Highest performance optimal sensor configurations.

To summarize, the optimized configuration had a very similar performance in four different cases (reflected in the Metric column). The most promising one (with the smallest metric value) was composed of one LIDAR pointing forward complemented by two laser rangefinders pointing at 10° sideways. That was the only configuration that resulted in only 8 close calls out of 40 maneuvers. The other three configurations, also with which no collisions registered, resulted in 9 close calls. It is also interesting to note that, in the

configurations listed in the last three lines of Table 3—despite having the exact values for failure, close call, and success rate—the metric function value varied. Recalling that not only does the metric function penalize breaching the safety and collision radii, but also accounts for the maximization of the minimum distance between the UAV and obstacles (see Equation (11)), then the lowest metric value of the two-RADAR and one-LIDAR solution reflected its ability to maintain a greater distance to the surrounding obstacles among these three configurations.

5. Conclusions

This work presents a comprehensive solution for enhancing the safety of small fixed-wing UAVs by addressing the critical issue of obstacle detection during flight. A set of select sensors, namely the ultrasonic sensor, laser rangefinder, LIDAR, and RADAR, were identified and further employed in modeling collision detection and avoidance simulations using the Potential Fields method.

To determine the best combination of sensors and their orientations, these simulations were used in an optimization study. The study revealed that relatively simple detection configurations can yield a high success rate in collision avoidance. While the ultrasonic sensor was found to be inadequate due to its limited range, the laser rangefinder benefited from a long range but had a restricted FOV. On the other hand, both the LIDAR and RADAR configurations proved to be the most promising options, offering not only a substantial range, but also a wide FOV. Based on the optimization study, the recommended multi-sensor configurations consist of a front-facing LIDAR accompanied by either two laser rangefinders pointing sideways at $\pm 10^\circ$ or two RADARs at $\pm 28^\circ$.

The two most promising solutions included a LIDAR, so it is important to note that the practical implementation of this type of sensor brings forth a set of challenges that must be carefully navigated for optimal performance in real-world scenarios. Cost is a critical factor influencing the feasibility of LIDAR-based obstacle detection systems. While LIDAR technology has advanced rapidly, the associated costs can be prohibitive, especially for smaller UAVs with limited budgets, so striking a balance between affordability and performance is crucial to ensure the widespread adoption of obstacle detection systems. Also, the compromise between sweep angle and speed is a nuanced consideration in optimizing collision avoidance systems since a wider sweep angle with faster sweeping speeds enhances coverage at the expense of possible missed detections, thus limiting the system's ability to identify threats.

While the particular solutions found here are strictly valid for the set of UAV flight performance parameters used, this work provides a generic comprehensive methodology for determining an optimized multi-sensor system configuration that holds great potential for enhancing the safety of small fixed-wing UAVs in flight.

Future work is twofold. Firstly, the extension to 3-D problems, both in terms of obstacle detection and collision avoidance maneuvers, adds an additional degree-of-freedom to the sensors' optimal orientation and elevation angle, as well as allows for climb and descent maneuvers. Lastly, the validation of the proposed multi-sensor system configurations implies challenging hardware and flight controller software implementations for flight testing. The collision avoidance method is then meant to run real time on board, and it is fed by live distance sensor data.

Author Contributions: Conceptualization, A.C.M.; methodology, A.C.M.; software, M.P.; validation, M.P.; formal analysis, M.P. and A.C.M.; investigation, M.P. and A.C.M.; resources, M.P. and A.C.M.; writing—original draft preparation, M.P.; writing—review and editing, A.C.M.; visualization, M.P.; supervision, A.C.M.; project administration, A.C.M.; funding acquisition, A.C.M. All authors have read and agreed to the published version of the manuscript.

Funding: This work was supported by Fundação para a Ciência e a Tecnologia (FCT) through IDMEC, under LAETA (project no. UIDB/50022/2020).

Data Availability Statement: The data presented in this study are available on request from the corresponding authors. The data are not publicly available due to privacy.

Acknowledgments: The authors acknowledge Nuno Alturas and Pedro Serrano for technical support.

Conflicts of Interest: The authors declare no conflict of interest. The funders had no role in the design of the study; in the collection, analyses, or interpretation of data; in the writing of the manuscript; or in the decision to publish the results.

Abbreviations

The following abbreviations are used in this manuscript:

2-D	Two-dimensional
3-D	Three-dimensional
FOV	Field of View
GA	Genetic Algorithm
LIDAR	Light Detection and Ranging
RADAR	Radio Detection and Ranging
S&A	Sense and Avoidance
UAV	Unmanned Aerial Vehicle

References

1. Mohsan, S.A.H.; Khan, M.A.; Noor, F.; Ullah, I.; Alsharif, M.H. Towards the Unmanned Aerial Vehicles (UAVs): A Comprehensive Review. *Drones* **2022**, *6*, 147. [[CrossRef](#)]
2. Polaris Market Research. Commercial UAV Market Share, Size, Trends & Industry Analysis Report By Type; By End-Use; By Region; Segment Forecast, 2021–2028. 2021. Report ID: PM1074. Available online: <https://www.polarismarketresearch.com/industry-analysis/commercial-uav-market> (accessed on 13 September 2023).
3. Altawy, R.; Youssef, M. Security, Privacy, and Safety Aspects of Civilian Drones: A Survey. *ACM Trans. Cyber-Phys. Syst.* **2016**, *1*, 1–25. [[CrossRef](#)]
4. Tahir, A.; Böling, J.; Haghbayan, M.H.; Toivonen, H.T.; Plosila, J. Swarms of Unmanned Aerial Vehicles—A Survey. *J. Ind. Inf. Integr.* **2019**, *16*, 100106. [[CrossRef](#)]
5. Yasin, J.N.; Haghbayan, M.H.; Yasin, M.M.; Plosila, J. Swarm formation morphing for congestion-aware collision avoidance. *Helyion* **2021**, *7*, e07840. [[CrossRef](#)]
6. Federal Aviation Administration. Next Generation Air Transportation System (NextGen). 2023. Available online: <https://www.faa.gov/nextgen> (accessed on 13 September 2023).
7. Federal Aviation Administration. Title 14 Code of Federal Regulations (CFR) Part 91.113 and RTCA. 2007. Available online: <https://www.govinfo.gov/content/pkg/CFR-2007-title14-vol1/html/CFR-2007-title14-vol1.htm> (accessed on 13 September 2023).
8. Yang, L.; Feng, X.; Zhang, J.; Shu, X. Multi-ray modeling of ultrasonic sensors and application for micro-UAV localization in indoor environments. *Sensors* **2019**, *19*, 1770. [[CrossRef](#)]
9. Schirrmann, M.; Hamdorf, A.; Giebel, A.; Gleiniger, F.; Pflanz, M.; Dammer, K.H. Regression kriging for improving crop height models fusing ultra-sonic sensing with UAV imagery. *Remote Sens.* **2017**, *9*, 665. [[CrossRef](#)]
10. Saunders, J.; Call, B.; Curtis, A.; Beard, R.; McLain, T. Static and dynamic obstacle avoidance in miniature air vehicles. In Proceedings of the Infotech@Aerospace, Arlington, VA, USA, 26–29 September 2005. [[CrossRef](#)]
11. Yin, D.; Wang, L. Individual mangrove tree measurement using UAV-based LiDAR data: Possibilities and challenges. *Remote Sens. Environ.* **2019**, *223*, 34–49. [[CrossRef](#)]
12. Skowron, M.; Chmielowiec, W.; Glowacka, K.; Krupa, M.; Srebro, A. Sense and avoid for small unmanned aircraft systems: Research on methods and best practices. *Proc. Inst. Mech. Eng. Part G J. Aerosp. Eng.* **2019**, *233*, 6044–6062. [[CrossRef](#)]
13. Lu, Y.; Xue, Z.; Xia, G.S.; Zhang, L. A survey on vision-based UAV navigation. *Geo-Spat. Inf. Sci.* **2018**, *21*, 21–32. [[CrossRef](#)]
14. Yasin, J.N.; Mohamed, S.A.S.; Haghbayan, M.H.; Heikkonen, J.; Tenhunen, H.; Plosila, J. Unmanned Aerial Vehicles (UAVs): Collision Avoidance Systems and Approaches. *IEEE Access* **2020**, *8*, 105139–105155. [[CrossRef](#)]
15. Mugnai, M.; Lose, M.T.; Herrera-Alarcon, E.P.; Baris, G.; Satler, M.; Avizzano, C.A. An Efficient Framework for Autonomous UAV Missions in Partially-Unknown GNSS-Denied Environments. *Drones* **2023**, *7*, 471. [[CrossRef](#)]
16. Aldao, E.; de Santos, L.M.G.; Gonzalez-Jorge, H. LiDAR Based Detect and Avoid System for UAV Navigation in UAM Corridors. *Drones* **2022**, *6*, 185. [[CrossRef](#)]
17. Langaker, H.A.; Kjerkreit, H.; Syversen, C.L.; Moore, R.J.; Holjhjem, O.H.; Jensen, I.; Morrison, A.; Transeth, A.A.; Kvien, O.; Berg, G.; et al. An autonomous drone-based system for inspection of electrical substations. *Int. J. Adv. Robot. Syst.* **2021**, *18*, 1–15. [[CrossRef](#)]
18. Karam, S.; Nex, F.; Chidura, B.T.; Kerle, N. Microdrone-Based Indoor Mapping with Graph SLAM. *Drones* **2022**, *6*, 352. [[CrossRef](#)]
19. Harvey, B.; O'Young, S. Acoustic Detection of a Fixed-Wing UAV. *Drones* **2018**, *2*, 4. [[CrossRef](#)]

20. Fraga-Lamas, P.; Ramos, L.; Mondéjar-Guerra, V.; Fernández-Caramés, T.M. A Review on IoT Deep Learning UAV Systems for Autonomous Obstacle Detection and Collision Avoidance. *Remote Sens.* **2019**, *11*, 2144. [[CrossRef](#)]
21. Xie, R.; Meng, Z.; Wang, L.; Li, H.; Wang, K.; Wu, Z. Unmanned Aerial Vehicle Path Planning Algorithm Based on Deep Reinforcement Learning in Large-Scale and Dynamic Environments. *IEEE Access* **2021**, *9*, 24884–24900. [[CrossRef](#)]
22. Alturas, N. Modeling and Optimization of an Obstacle Detection System for Small UAVs. Master’s Thesis, Instituto Superior Técnico, Universidade de Lisboa, Lisboa, Portugal, 2021.
23. Serrano, P. Optimization of Obstacle Detection for Small UAVs. Master’s Thesis, Instituto Superior Técnico, Universidade de Lisboa, Lisboa, Portugal, 2022.
24. Alturas, N.; Marta, A. Modeling and Optimization of an Obstacle Detection System for Small Fixed-wing UAV. In Proceedings of the Aerobest 2021—ECCOMAS Thematic Conference on Multidisciplinary Design Optimization of Aerospace Systems, Lisboa, Portugal, 21–23 July 2021; pp. 324–342. ISBN 978-989-99424-8-6.
25. MaxBotix. I2CXL-MaxSonar-EZ Datasheet. 2021. Available online: <https://maxbotix.com/pages/i2cxl-maxsonar-ez-datasheet> (accessed on 13 April 2023).
26. LightWare. Laser Rangefinder LW20/C Manual. 2020. Available online: <https://www.documents.lightware.co.za/LW20%20-%20LiDAR%20Manual%20-%20Rev%2012.pdf> (accessed on 13 April 2023).
27. LightWare. LiDAR SF45/B Guide. 2021. Available online: <https://support.lightware.co.za/sf45b/#/introduction> (accessed on 13 April 2023).
28. Ainstein. US-D1 Data Sheet. 2022. Available online: <https://ainstein.ai/wp-content/uploads/US-D1-Data-Sheet.pdf> (accessed on 13 April 2023).
29. Fayad, F.; Cherfaoui, V. Tracking objects using a laser scanner in driving situation based on modeling target shape. In Proceedings of the 2007 IEEE Intelligent Vehicles Symposium, Istanbul, Turkey, 13–15 June 2007; pp. 44–49. [[CrossRef](#)]
30. Grewal, M.S.; Andrews, A.P.; Bartone, C.G. *Kalman Filtering*, 2nd ed.; John Wiley & Sons, Inc.: New York, NY, USA, 2020; pp. 355–417. ISBN 0-471-26638-8.
31. Zhang, W.; Zhao, X.; Liu, Z.; Liu, K.; Chen, B. Converted state equation Kalman filter for nonlinear maneuvering target tracking. *Signal Process.* **2023**, *202*, 108741. [[CrossRef](#)]
32. Longbin, M.; Xiaoquan, S.; Yiyu, Z.; Kang, S.Z.; Bar-Shalom, Y. Unbiased converted measurements for tracking. *IEEE Trans. Aerosp. Electron. Syst.* **1998**, *34*, 1023–1027. [[CrossRef](#)]
33. Gageik, N.; Benz, P.; Montenegro, S. Obstacle Detection and Collision Avoidance for a UAV with Complementary Low-Cost Sensors. *IEEE Access* **2015**, *3*, 599–609. [[CrossRef](#)]
34. International Civil Aviation Organization. *Rules of the Air, Annex 2 to the Convention on International Civil Aviation*; International Civil Aviation Organization: Montreal, QC, Canada, 2005.
35. Alves, J. Path Planning and Collision Avoidance Algorithms for Small RPAS. Master’s Thesis, Instituto Superior Técnico, Universidade de Lisboa, Lisboa, Portugal, 2017.
36. Tekever. AR4 UAS Model. 2015. Available online: <https://www.tekever.com/models/ar4/> (accessed on 5 October 2022).
37. Rios, L.; Sahinidis, N. Derivative-free optimization: A review of algorithms and comparison of software implementations. *J. Glob. Optim.* **2013**, *56*, 1247–1293. [[CrossRef](#)]

Disclaimer/Publisher’s Note: The statements, opinions and data contained in all publications are solely those of the individual author(s) and contributor(s) and not of MDPI and/or the editor(s). MDPI and/or the editor(s) disclaim responsibility for any injury to people or property resulting from any ideas, methods, instructions or products referred to in the content.